Electronic Supplementary Material (ESI) for Journal of Materials Chemistry C.

Supporting Information

Efficient noise suppression via controlling the optical cavity in near-infrared organic photoplethysmography sensors

Zhao Yang,[a#] *Byung Gi Kim,*[b#] *Woongsik Jang*[a] *and Dong Hwan Wang*[*ab]

[a]School of Integrative Engineering, Chung-Ang University, 84 Heukseok-ro, Dongjak-gu, Seoul 06974, Republic of Korea

[b]Department of Intelligent Semiconductor Engineering Chung-Ang University 84 Heukseok-ro, Dongjak-gu, Seoul 06974, Republic of Korea

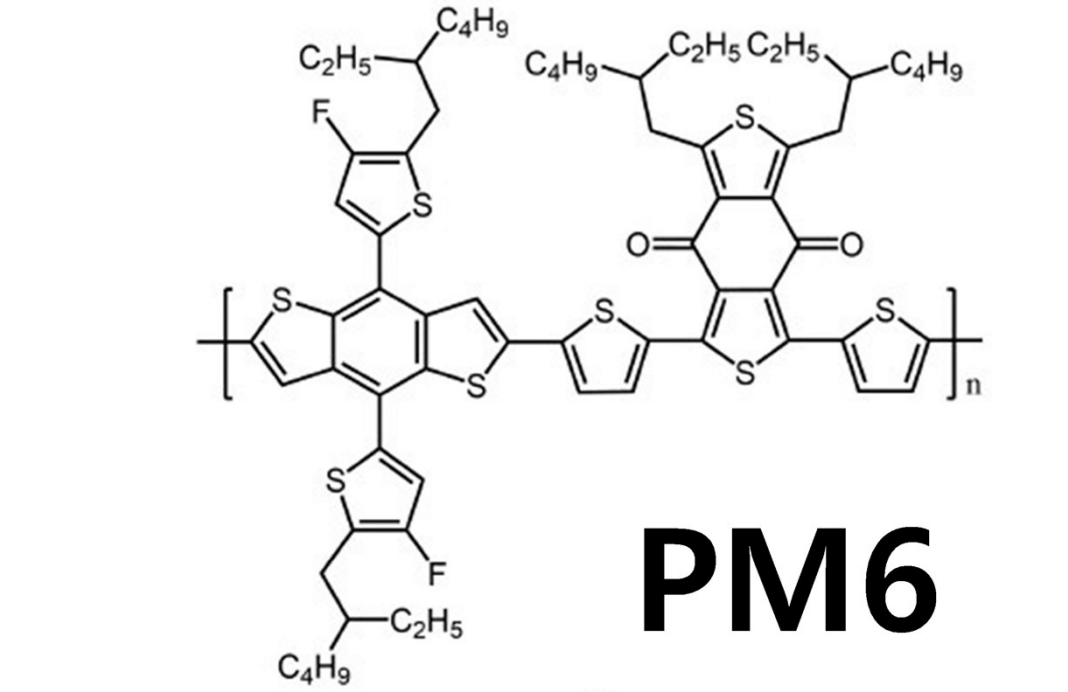

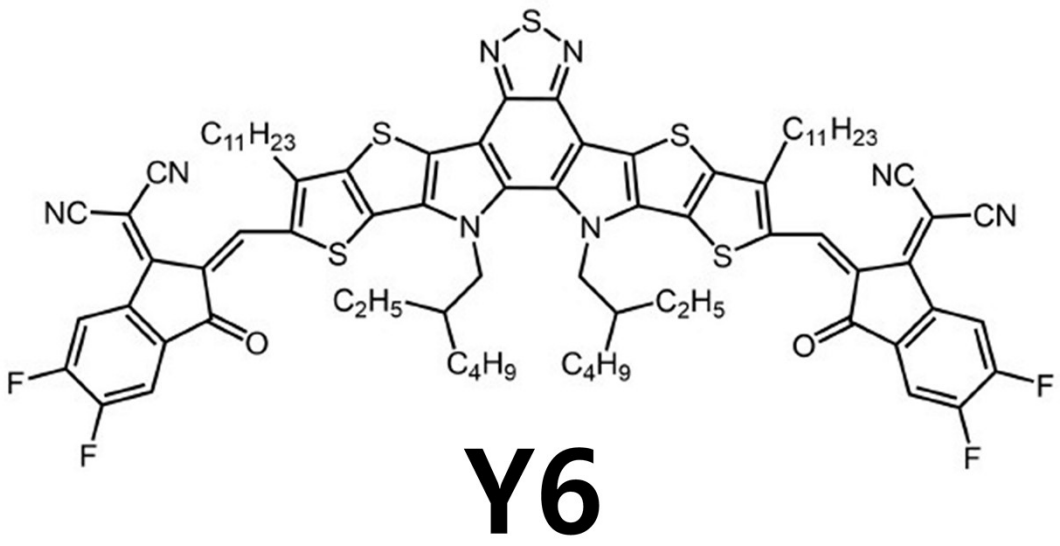

Fig. S1. Molecular structures of polymer donor PM6 and small-molecule acceptor Y6.

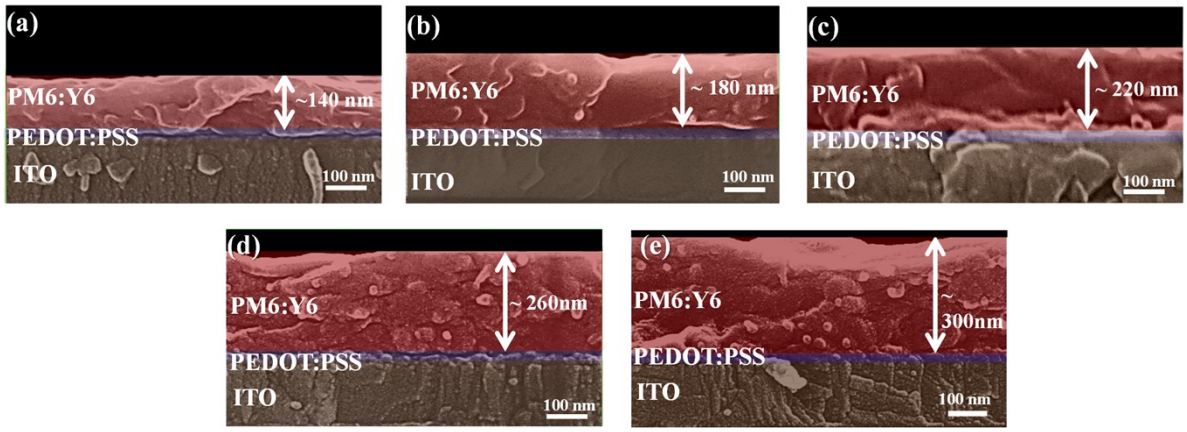

Fig. S2. Cross-sectional analysis of field emission scanning electron microscopy (FE-SEM) images for different thicknesses of the active layer: thickness-controlled ITO/PEDOT:PSS/PM6:Y6.

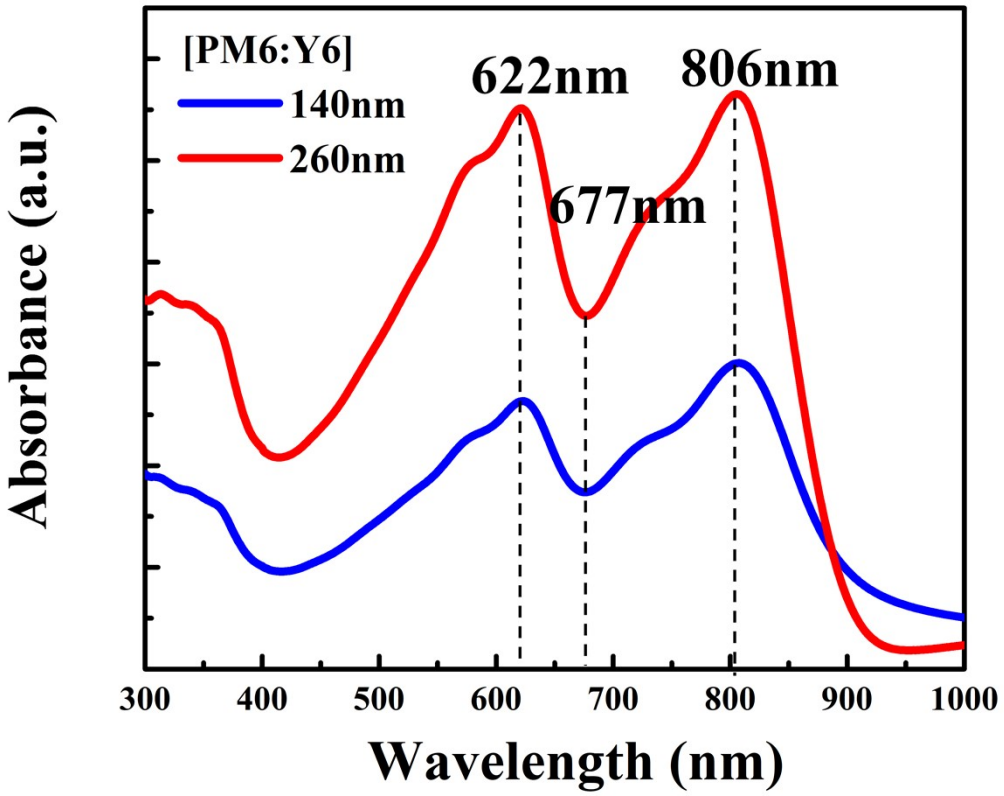

Fig. S3. Absorbance spectra characteristics of each PM6:Y6 film according to the different thicknesses of the PM6:Y6 active layer.

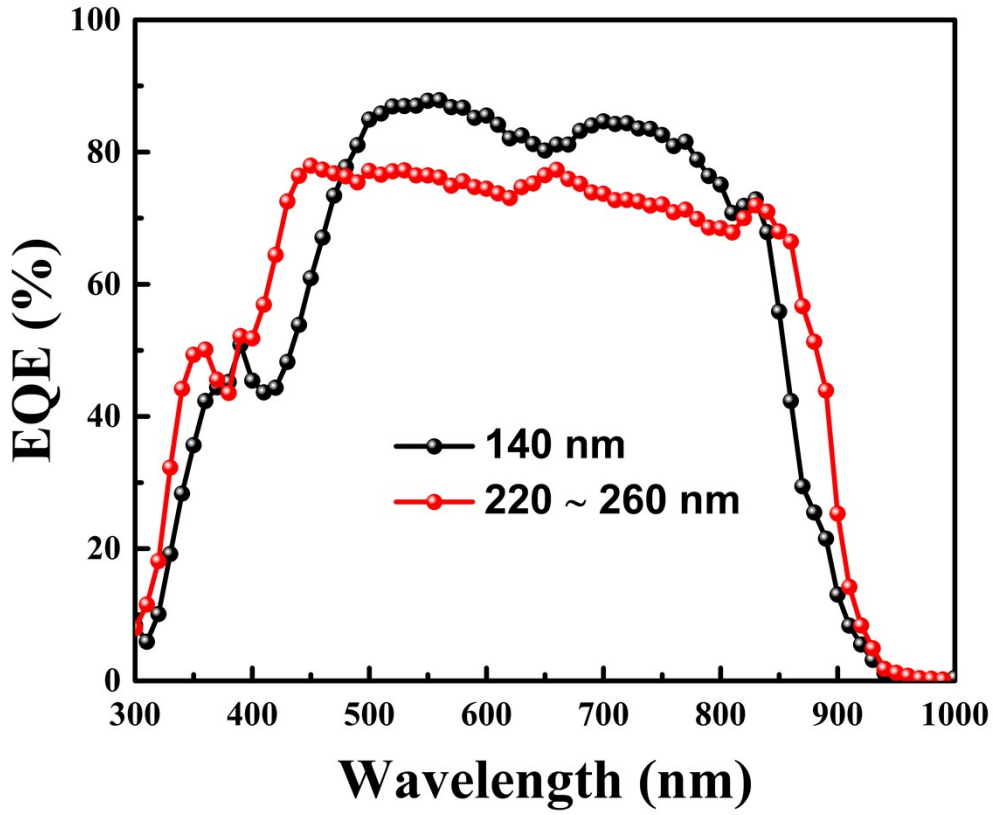

Fig. S4. EQE spectrum comparison of OPDs under each thickness with the reference and the other condition.

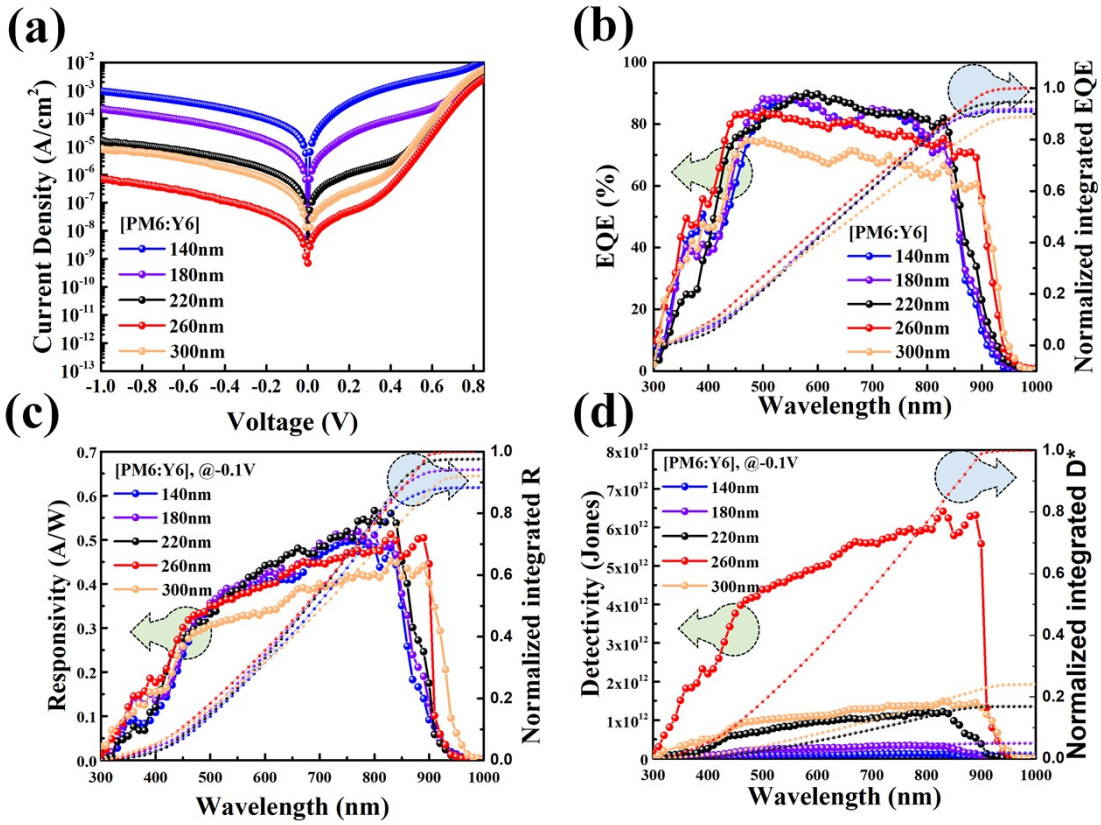

Fig. S5 (a) Dark J-V, (b) EQE, (c) responsivity (-0.1 V), (d) detectivity (-0.1 V), characteristics of all PM6:Y6 OPDs.

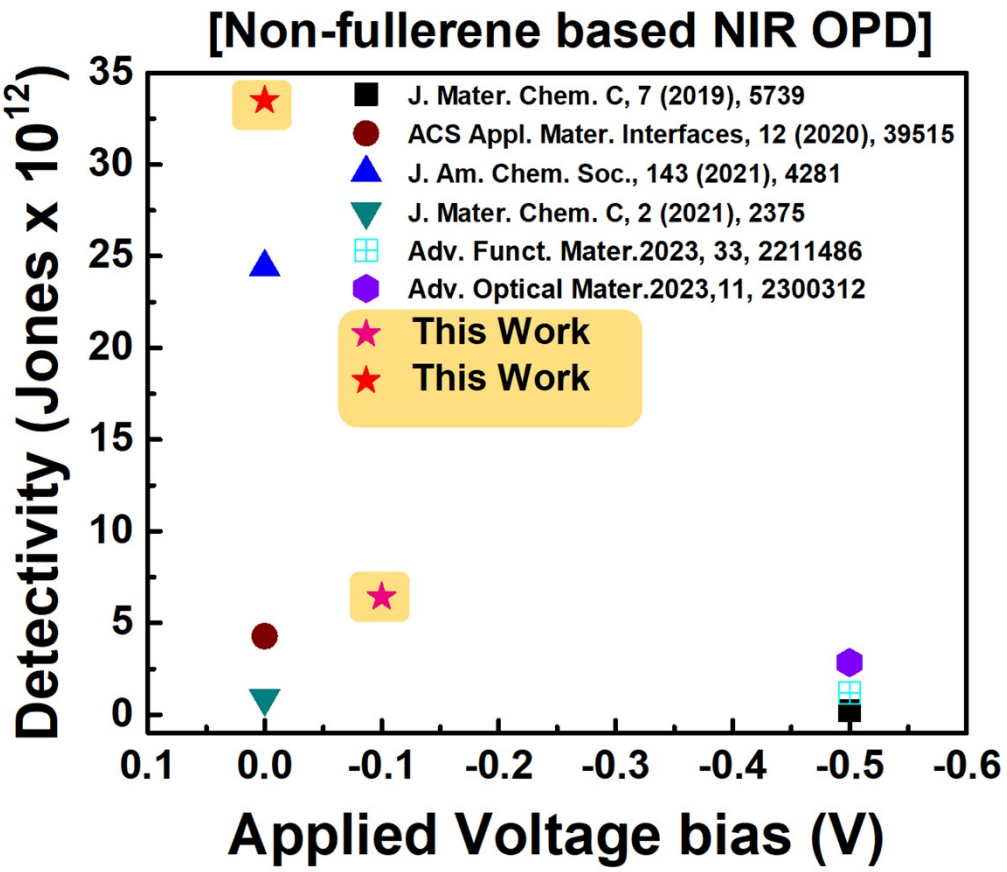

Fig. S6. Reported performance chart of non-fullerene based NIR OPDs.

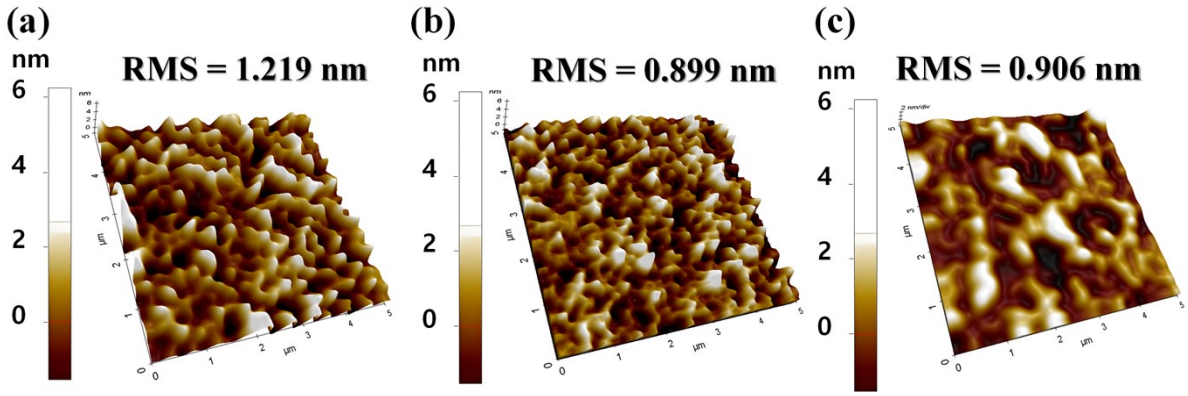

Figure S7. (a-c) Supplementary topography analysis of atomic force microscopy (AFM) 3D images of the PM6:Y6 with different thicknesses: (a) 180 nm, (b) 220 nm, (c) 300 nm.

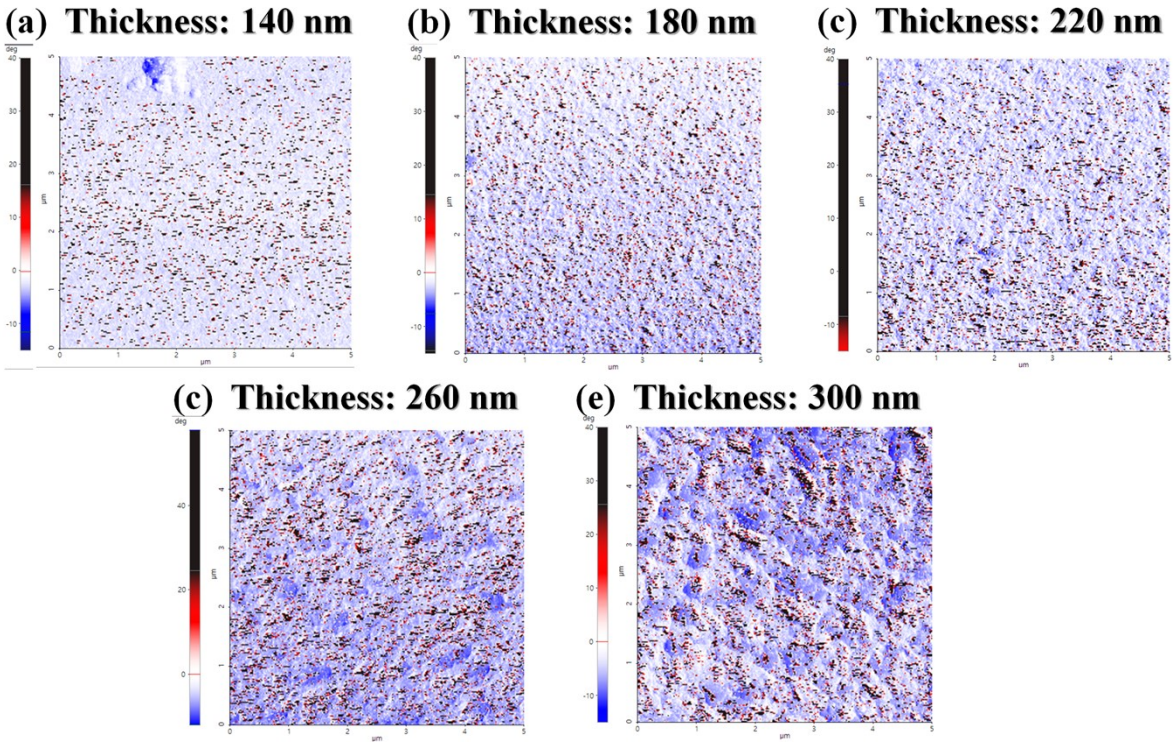

Figure S8. (a-e) Phase analysis of atomic force microscopy (AFM) images of the PM6:Y6 film depending on various thickness.

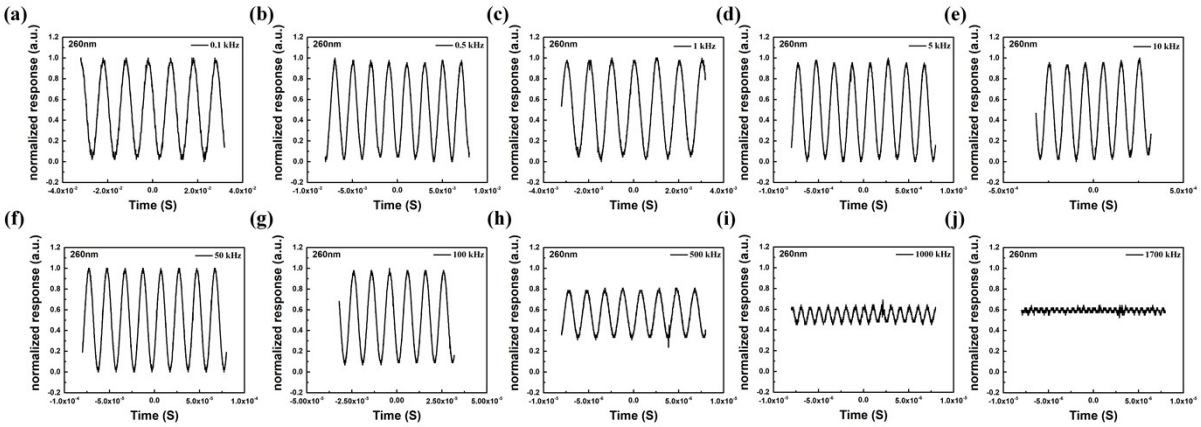

Fig. S9. (a-j) Normalized response characteristics of 140 nm PM6:Y6 OPD at 0 V; the frequency measurement range is from 0.1 to 1700 kHz.

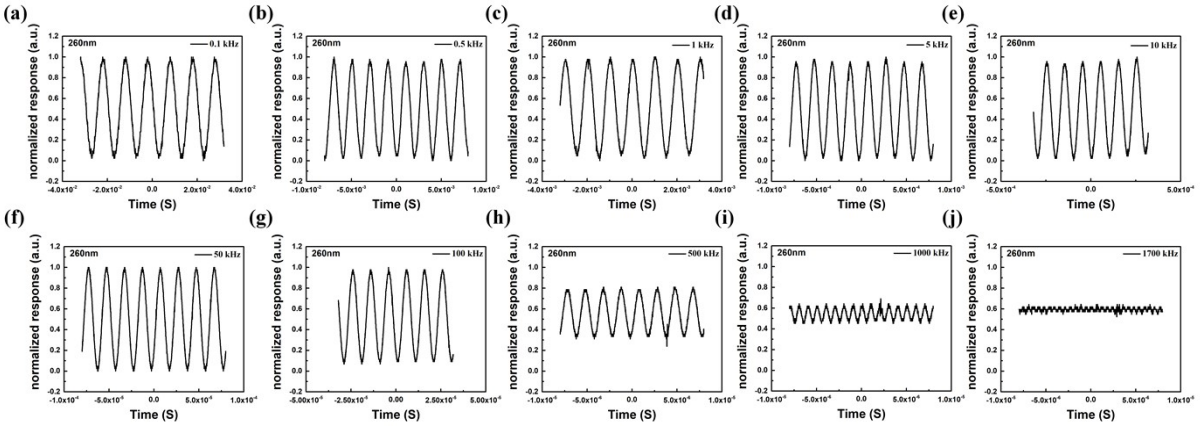

Fig. S10. (a-j) Normalized response characteristics of 260 nm PM6:Y6 OPD at 0 V; the frequency measurement range is from 0.1 to 1700 kHz.

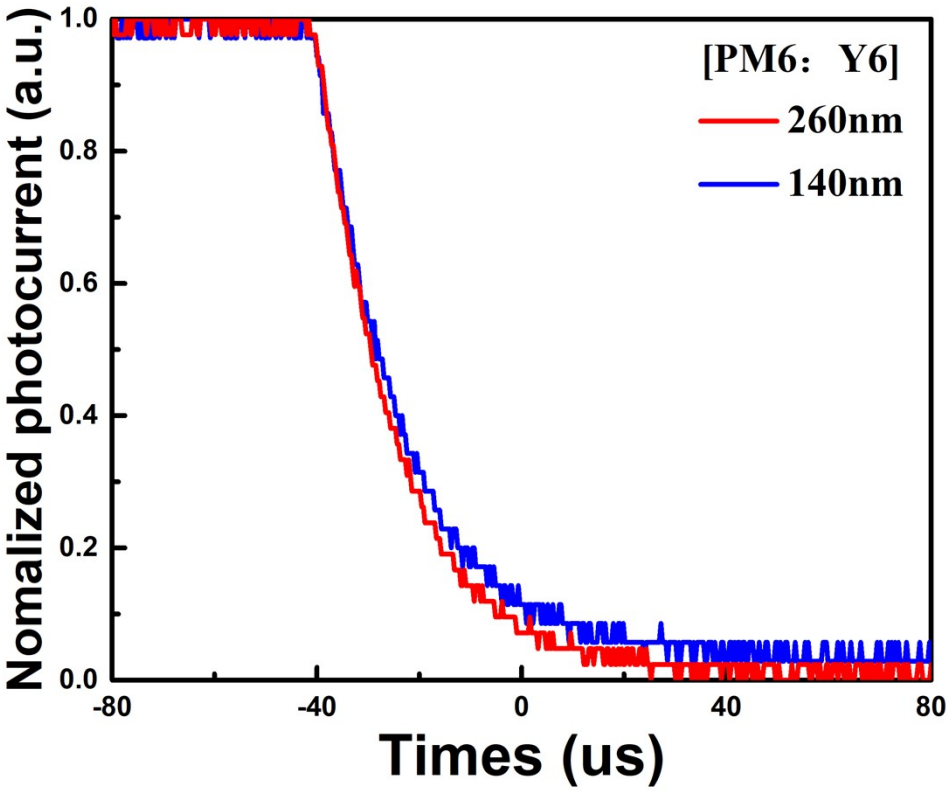

Fig. S11. Photoresponse times of thin and thick OPDs.

Table S1. Performance parameters of PM6:Y6-based devices according to active-layer thickness at −0.1 V.

Cell	J_D@−0.1 V （A/cm²）	R_{max} @−0.1 V (A/W)	D^*_{max} @−0.1 V (Jones)
140 nm	4.80×10^{-5}	0.498 @760 nm	1.27×10^{11} @760 nm
180 nm	7.13×10^{-6}	0.519 @770 nm	3.44×10^{11} @770 nm
220 nm	6.60×10^{-7}	0.566 @800 nm	1.23×10^{12} @800 nm
260 nm	1.99×10^{-8}	0.512 @830 nm	6.42×10^{12} @830 nm
300 nm	2.80×10^{-7}	0.452 @840 nm	1.49×10^{12} @840 nm

Table S2. Comparative performance chart of non-fullerene based NIR OPDs.

			J_{dark} (A/cm²)	D* (Jones)	Refs.
ITO/ZnO/P3HT:IDT-BOC/MoO3/Ag			6.3×10⁻⁶ (- 0.5 V)	2.1×10¹¹ (-0.5 V & 630 nm)	[4]
Thickness (nm)	**R_{sh} (KΩ)**	**C (F)**	**Shot noise@0V (AHz$^{-1/2}$)**	**Thermal noise (AHz$^{-1/2}$)**	**Total noise@0V (AHz$^{-1/2}$)**
ITO/ZnO/PTB7-Th:W1/MoOx/Ag			-	4.28×10¹² (0 V & 830 nm)	[2]
140	8.77	5.39×10⁻⁹	3.36×10⁻¹⁴	1.37×10⁻¹²	1.37×10⁻¹²
ITO/ZnO/PM6:PDTTIC-4F/MoO3/Ag			1.6×10⁻⁹ (0 V)	2.44×10¹³ (0 V & 920 nm)	[3]
140	14.42	4.65×10⁻⁹	1.76×10⁻¹⁴	1.07×10⁻¹²	1.07×10⁻¹²
ITO/PEDOT:PSS/PM6:O4TFIC/Phen-NaDPO/Ag			8.3×10⁻⁵ (-2 V)	9×10¹¹ (0 V & 915 nm)	[4]
ITO/ZnO/PTB7-Th:COTCN2/MoOx/Ag			1.08×10⁻⁷ (-0.5 V)	1.18×10¹² (-0.5 V & 1000 nm)	[5]
ITO/ZnO/PTB7-Th:COB/MoOx/Ag			2.26×10⁻⁷ (-0.5 V)	2.84×10¹¹ (-0.5 V & 915 nm)	[6]
ITO/PEDOT:PSS/PM6:Y6/PDINN/Ag			1.99×10⁻⁸ (-0.1 V)	6.42×10¹² (-0.1 V & 830 nm)	This work
			7.07×10⁻¹⁰ (0 V)	3.35×10¹³ (0 V & 830 nm)	

260	37.64	2.37×10^{-9}	1.35×10^{-14}	6.61×10^{-13}	6.61×10^{-13}
260	150.33	8.30×10^{-10}	5.82×10^{-15}	3.31×10^{-13}	3.31×10^{-13}

Table S3. Impedance-related parameters and noise component analysis of PM6:Y6 devices based on different active-layer thicknesses.

Table S4. Hole-only SCLC parameters of PM6:Y6 devices based on different active-layer thicknesses.

Hole-only devices: ITO/PEDOT:PSS/PM6:Y6 (140 & 260 nm)/MoO_3/Ag

Thickness (nm)	V_{TFL} (V)	N_{trap} ($\#cm^{-3}$)
140	0.94	2.09×10^{16}
260	0.64	4.13×10^{15}

Table S5. Electron-only SCLC parameters of PM6:Y6 devices based on different active-layer thicknesses.

Electron-only devices: ITO/ZnO/PM6:Y6 (140 & 260 nm)/PDINN/Ag

Thickness (nm)	V_{TFL} (V)	N_{trap} ($\#cm^{-3}$)
140	0.86	1.91×10^{16}
260	0.75	4.84×10^{15}

References:

1 Y. Jinde, X. Sui, G. Lu, L. Lv, J. Yu, J. Wu, X. Dong, X. Liu, A. Peng, H. Huang, Significant enhancement of responsivity of organic photodetectors upon molecular engineering, J. Mater. Chem. C. 7 (2019) 5739. https://doi.org/10.1039/C9TC00576E.

2 T.J. Wen, D. Wang, L. Tao, Y. Xiao, Y.D. Tao, Y. Li, X. Lu, Y. Fang, C.Z. Li, H. Chen, D. Yang, Simple Near-Infrared Electron Acceptors for Efficient Photovoltaics and Sensitive Photodetectors, ACS Appl. Mater. Interfaces. 12 (2020) 39515–39523. https://doi.org/10.1021/ACSAMI.0C12100.

3 Y. Chen, Y. Zheng, Y. Jiang, H. Fan, X. Zhu, Carbon-Bridged 1,2-Bis(2-Thienyl)ethylene: An Extremely Electron Rich Dithiophene Building Block Enabling Electron Acceptors with Absorption above 1000 nm for Highly Sensitive NIR Photodetectors, J. Am. Chem. Soc. 143 (2021) 4281–4289. https://doi.org/10.1021/JACS.0C12818

4 M. Babics, H. Bristow, W. Zhang, A. Wadsworth, M. Neophytou, N. Gasparini, I. McCulloch, Non-fullerene-based organic photodetectors for infrared communication, J. Mater. Chem. C. 9 (2021) 2375–2380. https://doi.org/10.1039/D0TC05341D.

5 J.W. Ha, H.J. Eun, B. Park, H. Ahn, D.R. Hwang, Y.S. Shim, J. Heo, C. Lee, S.C. Yoon, J.H. Kim, S.J. Ko, Effect of Cyano Substitution on Non-Fullerene Acceptor for Near-Infrared Organic Photodetectors above 1000 nm, Adv. Funct. Mater. 33 (2023) 2211486. https://doi.org/10.1002/ADFM.202211486.

6 U.H. Lee, B. Park, S. Rhee, J.W. Ha, D.R. Whang, H.J. Eun, J.H. Kim, Y. Shim, J. Heo, C. Lee, B.J. Kim, S.C. Yoon, J. Lee, S.J. Ko, Achieving Highly Sensitive Near-Infrared Organic Photodetectors using Asymmetric Non-Fullerene Acceptor, Adv. Opt. Mater. 11 (2023) 2300312. https://doi.org/10.1002/ADOM.202300312.